J Appl Electrochem (2010) 40:783–789
DOI 10.1007/s10800-009-0057-2

ORIGINAL PAPER

# Preparation and electrochemical performance of Li-rich layered cathode material, $Li[Ni_{0.2}Li_{0.2}Mn_{0.6}]O_2$, for lithium-ion batteries

**Feng Wu · Huaquan Lu · Yuefeng Su · Ning Li · Liying Bao · Shi Chen**

Received: 3 September 2009 / Accepted: 8 December 2009 / Published online: 24 December 2009


**Abstract** The Li-rich layered cathode material, $Li[Ni_{0.2}Li_{0.2}Mn_{0.6}]O_2$, was synthesized via a "mixed oxalate" method, and its structural and electrochemical properties were compared with the same material synthesized by the sol–gel method. X-ray diffraction (XRD) shows that the synthesized powders have a layered $O_3$–$LiCoO_2$-type structure with the *R-3m* symmetry. X-ray photoelectron spectroscopy (XPS) indicates that in the above material, Ni and Mn exist in the oxidation states of +2 and +4, respectively. The layered material exhibits an excellent electrochemical performance. Its discharge capacity increases gradually from the initial value of 228 mA $hg^{-1}$ to a stable capacity of over 260 mA $hg^{-1}$ after the 10th cycle. It delivers a larger capacity of 258 mA $hg^{-1}$ at the 30th cycle. The d*Q*/d*V* curves suggest that the increasing capacity results from the redox-reaction of $Mn^{4+}/Mn^{3+}$.

**Keywords** Lithium-ion batteries · "Mixed oxalate" method · Cathode materials · Layered structure

**Electronic supplementary material** The online version of this article (doi:10.1007/s10800-009-0057-2) contains supplementary material, which is available to authorized users.

F. Wu · H. Lu · Y. Su (✉) · N. Li · L. Bao · S. Chen
School of Chemical Engineering and Environment, Beijing Institute of Technology, 100081 Beijing, China
e-mail: suyuefeng@bit.edu.cn

F. Wu · H. Lu · Y. Su · N. Li · L. Bao · S. Chen
National Development Center of High Technology Green Materials, 100081 Beijing, China

## 1 Introduction

Recently, the solid solutions between $Li[Li_{1/3}Mn_{2/3}]O_2$ (i.e., $Li_2MnO_3$) and $LiMO_2$ (M = Co [1], Cr [2, 3], $Ni_{1/2}Mn_{1/2}$ [4, 5] or $Ni_{1/3}Co_{1/3}Mn_{1/3}$ [6]) have emerged as promising cathode materials for lithium-ion batteries. Among these integrated materials being developed, much attention has been paid to $xLi[Li_{1/3}Mn_{2/3}]O_2 \cdot (1-x)LiNi_{1/2}Mn_{1/2}O_2$, which can also be written in layered notation as $Li[Li_{(1-2x)/3}Ni_xMn_{(2-x)/3}]O_2$ ($0 \le x \le 0.5$), for they have retained the high capacity of $LiNi_{1/2}Mn_{1/2}O_2$ and the good thermal stability of $Li_2MnO_3$. However, this kind of materials usually exhibits a large irreversible capacity at the first cycle when charged to high potentials (4.6–4.8 V), which is considered to be caused by the irreversible removal of $Li^+$ and $O^{2-}$ as "$Li_2O$" from the lattice [7, 8]. Fortunately, this large irreversible capacity appears to be found only in the first cycle, and in the following cycles, $Li^+$ intercalation and deintercalation are reversible. These cathode materials show good cycling behavior and deliver a stable specific capacity of about 250 mA $hg^{-1}$, which have an obvious advantage over the commercially used $LiCoO_2$ cathode.

The Li $[Li_{(1-2x)/3}Ni_xMn_{(2-x)/3}]O_2$ ($0 \le x \le 0.5$) compounds were conventionally prepared by a sol–gel method [4, 9], or a "mixed hydroxide" method [10–13]. The sol–gel method was an extensively used method, which can produce the layered Li–Ni–Mn–O compounds with a high homogeneity. It is worth noting that this method is time consuming, particularly when careful aging and drying are required, and this definitely limits large scale production. The "mixed hydroxide" method is another widely adopted method, which uses the co-precipitated Ni and Mn hydroxides to mix with lithium hydroxide together and then heat-treats the mixed compounds into $Li[Li_{(1-2x)/3}Ni_xMn_{(2-x)/3}]O_2$ ($0 \le x \le 0.5$). However, the homogeneous hydroxides

$Ni_xMn_{1-x}(OH)_2$ are difficult to obtain because $Mn(OH)_2$ in alkaline condition can be easily oxidized by air [14], and inert gas protection was often applied to get homogeneous hydroxides [15, 16].

In this study, we successfully synthesized $Li[Ni_{0.2}Li_{0.2}Mn_{0.6}]O_2$ (i.e., $Li[Li_{(1-2x)/3}Ni_xMn_{(2-x)/3}]O_2$, $x = 0.2$) by using the "mixed oxalate" method. In this method, a homogeneous mixed oxalate of $NiC_2O_4$ and $MnC_2O_4$ obtained from oxalate co-precipitation was used as the precursor, and by heat-treating the mixture of the precursor and $LiNO_3$, the high electrochemical active $Li[Ni_{0.2}Li_{0.2}Mn_{0.6}]O_2$ was obtained. Compared with the "mixed hydroxide" method, one advantage of the present method is that during the process of oxalate co-precipitation, the pH of the solution can be controlled in a neutral range, and, thus, the divalent Mn would not be oxidized easily and it does not need inert gas protection. In this article, we compared the electrochemical behavior of $Li[Ni_{0.2}Li_{0.2}Mn_{0.6}]O_2$ synthesized by the "mixed oxalate" method with the one by the sol–gel method. The results show that $Li[Ni_{0.2}Li_{0.2}Mn_{0.6}]O_2$ materials synthesized by the "mixed oxalate" method have a comparable electrochemical property with or even better than the electrochemical property of the sample synthesized by the sol–gel method. In view of the complex and time-consuming nature of processes by the sol–gel method, the "mixed oxalate" method is considered as a better choice to synthesize $Li[Ni_{0.2}Li_{0.2}Mn_{0.6}]O_2$, producing high electrochemical performance. Furthermore, the latter synthesis method can be easily controlled and reproduced, thereby being very efficient for industrial applications.

## 2 Experimental

Li-rich layered $Li[Ni_{0.2}Li_{0.2}Mn_{0.6}]O_2$ samples were synthesized by the "mixed oxalate" method and the sol–gel method. The sample synthesized by the "mixed oxalate" was obtained as follows: nickel nitrate and manganese nitrate were dissolved in distilled water. Ammonium oxalate was dissolved in another cup of distilled water to get aqueous solutions. The two solutions were added slowly into a reactor, in which distilled water was under vigorous stirring. During the precipitation, the pH of the reaction solution was adjusted to 7.0 by adding $NH_3{\cdot}H_2O$. The resulting sediment was mixed with $LiNO_3$ in stoichiometric proportions and preliminarily annealed at 450 °C for 5 h in air. Then, the precursors were pressed into pellets and heat-treated at 900 °C for 12 h in air followed with quenching in two copper plates. For the sol–gel method, the synthesis procedure is the same as in the previous literatures [9]. Stoichiometric amounts of lithium acetate, nickel acetate, and manganese acetate were dissolved in distilled water. Citric acid was added into the solution under vigorous stirring to form a high viscous gel. The gel was decomposed at 450 °C in air for 5 h and ground after cooling. The decomposed mixture was pressed into pellets and calcined at 900 °C in air for 12 h followed by quenching in two copper plates.

Inductively coupled plasma atomic emission spectroscopy (ICP-AES, Thermo, IRIS Advantage) method was used to analyze the chemical compositions of the samples. Powder X-ray diffraction (XRD) was performed on Rigaku Dmax/2400 diffractometer with Cu $K_\alpha$ radiation. The collected intensity data of XRD were analyzed by the Rietveld refinement using the Fullprof program [17]. The morphology and the particle size of the samples were observed by scanning electron microscope (FEI QUANTA 6000). X-ray photoelectron spectroscopy (XPS) of the samples were obtained using PHI Quantera spectrometer with monochromatic Al $K_\alpha$ radiation ($h_v = 1{,}486.6$ eV) to determine chemical valence state of transition elements. Binding energies were charge corrected using the C 1s peak (284.8 eV).

Electrochemical properties of the synthesized materials were examined using galvanostatic cycling with coin cells (2025) at the room temperature. The cathode mixtures consisting of 75 wt% metal oxide powder, 18 wt% acetylene black, and 7 wt% polyvinylidene difluoride (PVDF) binder were spread on aluminum foil. 1 M $LiPF_6$ in a 1:1 ethylene carbonate (EC)/dimethyl carbonate (DMC) was used as the electrolyte, lithium foil as the anode, and Celgard 2400 membrane as the separator. Galvanostatic charge–discharge tests were performed by LAND battery test system (Wuhan China).

## 3 Results and discussions

### 3.1 Powder characterization

In order to determine the chemical composition of the two samples, an ICP-AES method was used here. The results in weight percent were converted to atomic percent and then ultimately converted to stoichiometry. The chemical composition of the samples obtained from the sol–gel method and the oxalate precursor method are determined to be $Li_{1.22}Ni_{0.18}Mn_{0.6}O_{1.96}$ and $Li_{1.22}Ni_{0.19}Mn_{0.6}O_{1.98}$, respectively, which agrees with the desired composition within experimental uncertainty.

Rietveld refinement results of X-ray diffraction patterns of $Li[Ni_{0.2}Li_{0.2}Mn_{0.6}]O_2$ powders synthesized by the "mixed oxalate" method and the sol–gel method are given in Fig. 1. Some weak diffraction peaks between 20° and 25° of $2\theta$ can be observed in the XRD patterns of the two samples, which are considered to be caused by the short-range superlattice ordering of Li, Ni, and Mn in the transition metal

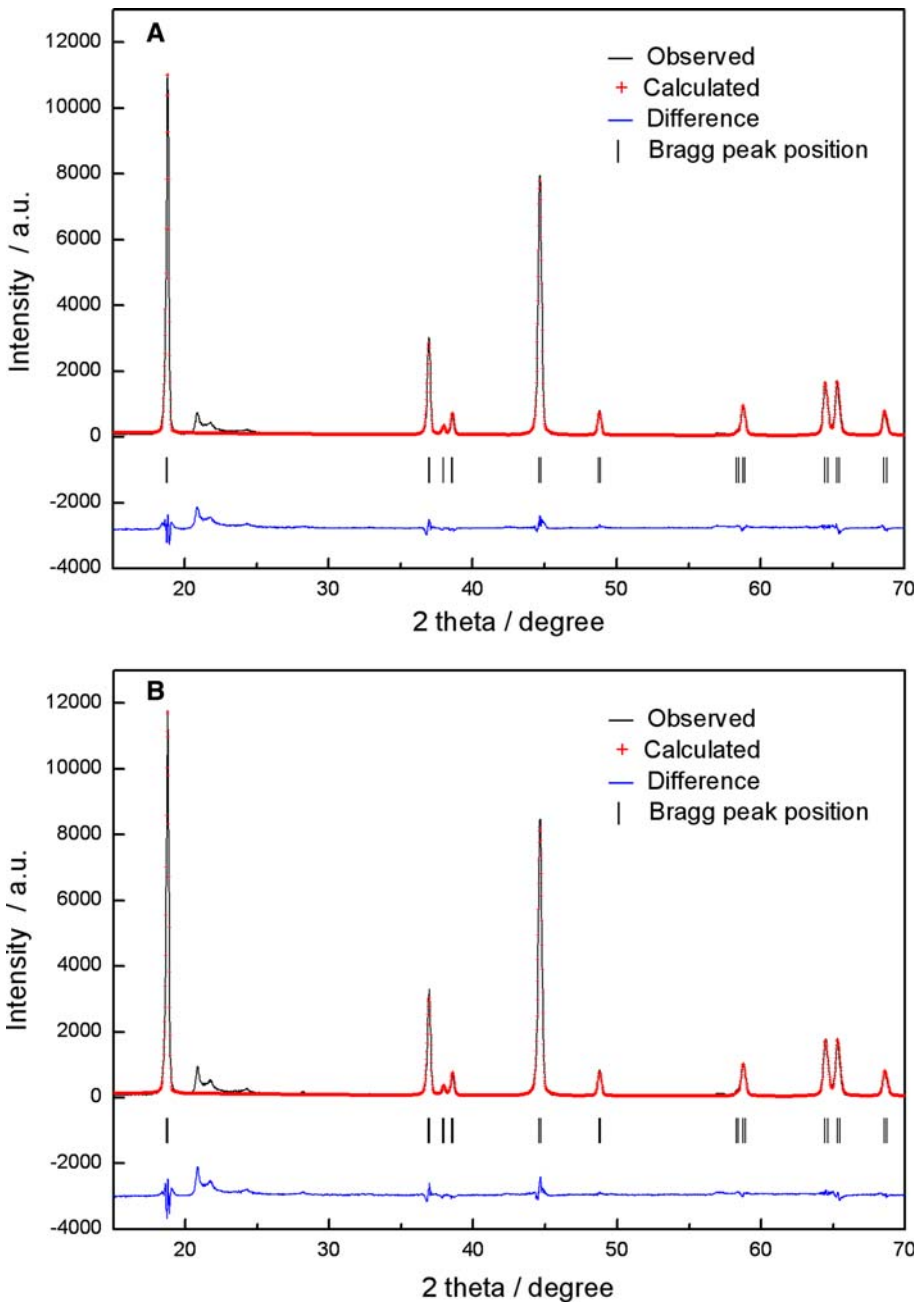


**Fig. 1** Rietveld refinement of X-ray diffraction patterns of $Li[Ni_{0.2}Li_{0.2}Mn_{0.6}]O_2$ synthesized by different methods: (**A**) "mixed oxalate" method; (**B**) sol–gel

layer [4]. These peaks can be indexed to *C2/m* space group that characterizes $Li_2MnO_3$ [13, 18]. Except for the weak and broad peaks between 20° and 25°, all the strong diffraction peaks can be simply indexed to the $O_3$–$LiCoO_2$-type structure with the *R-3m* symmetry, as reported in the literatures [8, 9, 19–21] because of the remarkable structural compatibility of layered $Li_2MnO_3$ and $LiNi_{1/2}Mn_{1/2}O_2$. The clear splitting between the (006)/(102) and (108)/(110) peaks in the XRD patterns of the two samples indicates that the synthesized powers have good layered characteristics [22]. Here, Rietveld refinements were carried out for the samples by assuming the space group of *R-3m* and supposing that $Ni^{2+}$ located at the 3b sites can be exchanged with $Li^+$ occupied at the 3a site due to the similarity of their ionic radii ($Li^+$: 0.69 Å; $Ni^{2+}$: 0.76 Å). As shown in Fig. 1, the calculated patterns are in good agreement with the observed patterns. The refinement results and reliability factors are summarized in Table 1. It was found that the lattice parameters *a* and *c* of the two samples are almost the same, but the Li/Ni disorder in the "mixed oxalate" sample is a little smaller than that of the sol–gel sample.

Figure 2 is the SEM images of the $Li[Ni_{0.2}Li_{0.2}Mn_{0.6}]O_2$ samples. All the particles of the two samples have the same morphology looking like rock-shaped grains. The average

**Table 1** X-ray Rietveld refinement results of $Li[Ni_{0.2}Li_{0.2}Mn_{0.6}]O_2$ synthesized by "mixed oxalate" method and sol–gel methods

| Synthesis route | Reliability factor (%) | Lattice parameters (Å) | *c*/*a* | Li/Ni disorder (%) |
|---|---|---|---|---|
| "Mixed oxalate" | $R_p = 9.11$ | $a = 2.8580$ | 4.984 | 2.96 |
| | $R_{wp} = 14.5$ | $c = 14.2461$ | | |
| | $R_{exp} = 5.3$ | | | |
| Sol–gel | $R_p = 9.52$ | $a = 2.8570$ | 4.985 | 3.22 |
| | $R_{wp} = 14.8$ | $c = 14.2427$ | | |
| | $R_{exp} = 5.15$ | | | |

diameter of the particles was found to be less than 500 nm, and some of the particles agglomerate together to form big particles. The extent of particle agglomeration of the sol–gel sample is a little higher than that of the "mixed oxalate" sample. In general, a lower extent agglomeration and a more uniform particle distribution can lead to a better electrochemical performance. Thus, the sample synthesized by "mixed oxalate" method may have a better electrochemical performance, which is coincident with the charge–discharge testing results.

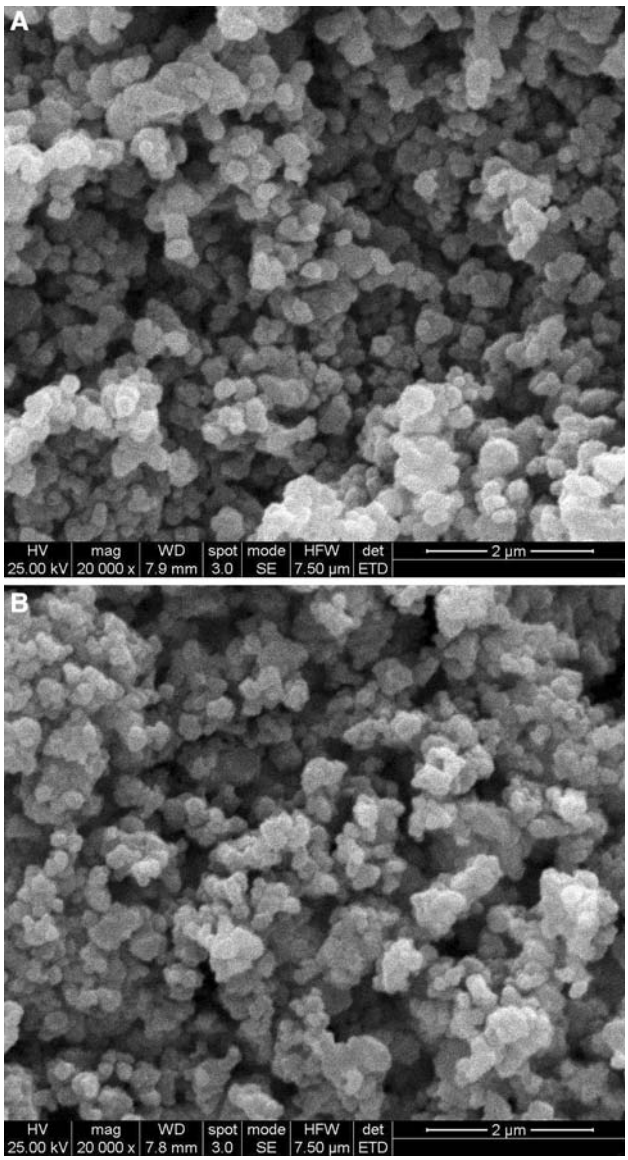


**Fig. 2** SEM images of $Li[Ni_{0.2}Li_{0.2}Mn_{0.6}]O_2$ synthesized by different methods: (**A**) "mixed oxalate" method; (**B**) sol–gel

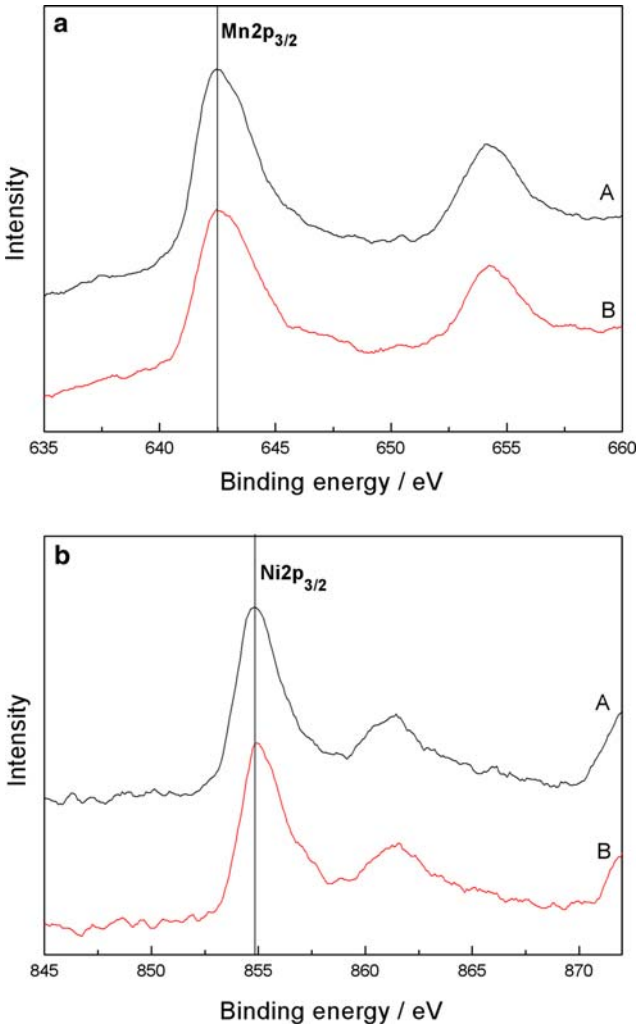


**Fig. 3** XPS spectra of Mn 2p (**a**) and Ni 2p (**b**) in $Li[Ni_{0.2}Li_{0.2}Mn_{0.6}]O_2$ synthesized by different methods: (**A**) "mixed oxalate" method; (**B**) sol–gel

$Li[Ni_{0.2}Li_{0.2}Mn_{0.6}]O_2$ powders are characterized by XPS to confirm the oxidation states of the transition metals. The Mn 2p and Ni 2p XPS spectra for the $Li[Ni_{0.2}Li_{0.2}Mn_{0.6}]O_2$ powder are shown in Fig. 3. The binding energies of the transition metals in the two samples synthesized by different methods are almost the same. The binding energy of Ni $2p_{3/2}$ is 854.8 eV, which can be attributed to $Ni^{2+}$ according to the previous XPS studies [23, 24]. Similarly, the binding energy of Mn $2p_{3/2}$ is 642.5 eV, which is very close to that (642.4 eV) of Mn $2p_{3/2}$ in $\lambda$-$MnO_2$ [25]. Therefore, it is believed that the valence of Mn in the two samples is +4.

### 3.2 Electrochemical performances

The electrochemical charge–discharge measurements of the samples were carried out using Li metal as the anode between 2.5 and 4.8 V at a constant current density of 0.1 C rate. Figure 4 shows the initial charge–discharge curves and differential capacity plots versus voltage for lithium half-cells using $Li[Ni_{0.2}Li_{0.2}Mn_{0.6}]O_2$ synthesized by the two different methods. The sample A (synthesized by the "mixed oxalate" method) shows a discharge capacity of 228 mA $hg^{-1}$, and its irreversible capacity is found to be 70.7 mA $hg^{-1}$, around 23.6% of its first charge capacity, whereas the sample B (synthesized by the sol–gel method) shows a lower discharge capacity of 213.6 mA $hg^{-1}$ and a higher irreversible capacity of 83.1 mA $hg^{-1}$ (28% of its first charge capacity). It can be clearly seen from Fig. 4 that the initial charging curves of both samples show two plateaus: one is observed below 4.5 V (a–b), and the other is above 4.5 V (b–c). At the former plateau, the voltage increases monotonically, corresponding to the oxidation of $Ni^{2+}$ to $Ni^{4+}$, until the potential reaches 4.5 V, at which all Ni exist in the +4 oxidation state [8]. Accordingly, the two small oxidation peaks below 4.5 V observed from their differential capacity plots of the two samples can be probably attributed to the redox-reaction of $Ni^{2+}/Ni^{3+}$ and $Ni^{3+}/Ni^{4+}$, respectively. The latter plateau starts from 4.5 V, and big corresponding oxidation peaks can be observed from their differential capacity plots, resulting from the electrochemical removal of $Li_2O$ from the structure [8], which is responsible for the big irreversible capacity. According to Lu et al. [7], the oxidation peak of $Mn^{3+}/Mn^{4+}$ occurs below 3.5 V. No redox-reaction peaks below 3.5 V were found in the first charge curves of the two samples, indicating that Mn ions in the two samples are $Mn^{4+}$, which is in agreement with the XPS results. Although the initial charging curves of the two samples seem to be the same, some distinct differences in the reduction part of the differential capacity plots of the two samples can be observed. Apart from the reduction peaks between 3.5 and 4.5 V corresponding to the reduction reaction of $Ni^{4+}$ to $Ni^{2+}$ [19], another larger reduction peak below 3.5 V appears on the differential capacity plots of the sample synthesized by the "mixed oxalate" method, which can be possibly ascribed to the reduction of Mn in the cathode from +4 to +3 [8, 26, 27]. This result means that partial Mn does participate in the electrochemical reactions when the sample (synthesized by the "mixed oxalate" method) is discharged to 2.5 V.

The cycling performances of $Li[Ni_{0.2}Li_{0.2}Mn_{0.6}]O_2$ synthesized by the "mixed oxalate" method and the sol–gel method are compared in Fig. 5. Interestingly, the discharge capacities of the two samples do not fade while

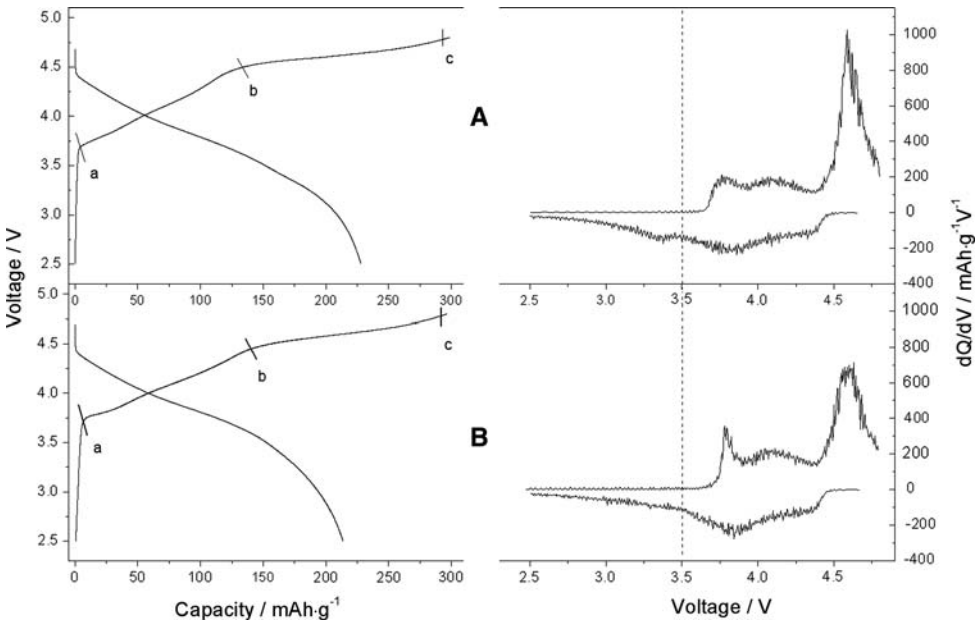


**Fig. 4** The initial charge–discharge curves and differential capacity plots versus voltage of $Li[Ni_{0.2}Li_{0.2}Mn_{0.6}]O_2$ synthesized by (**A**) "mixed oxalate" method and (**B**) sol–gel method in the voltage range of 2.5–4.8 V at 0.1 C

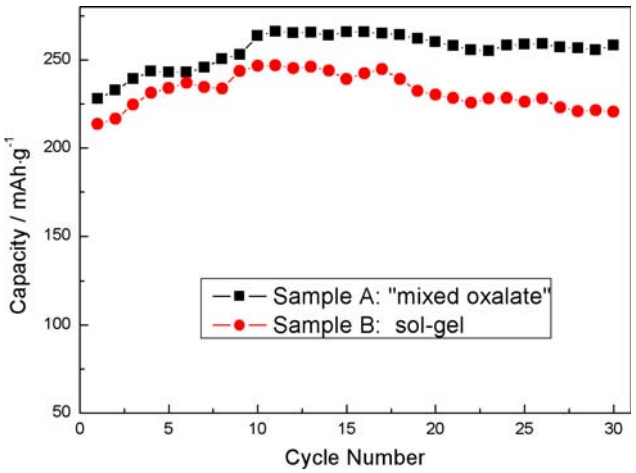


**Fig. 5** Discharge capacities as a function of the cycle number for $Li[Ni_{0.2}Li_{0.2}Mn_{0.6}]O_2$ synthesized by (**A**) "mixed oxalate" method and (**B**) sol–gel method cycled at 0.1 C in the voltage range of 2.5–4.8 V

cycling; on the contrary, they gradually increase as the charge and discharge cycles go on, and become stable after 10 cycles. Similar results can also be found in previous literatures [26, 27]. The reason why the capacity increases with the cycle will be discussed later. The sample A (synthesized by the "mixed oxalate" method) exhibits a discharge capacity of about 230 mA $hg^{-1}$ at the initial cycle, and the reversible capacity climbs to more than 260 mA $hg^{-1}$ after 10 cycles. It delivers a larger capacity of 258 mA $hg^{-1}$ at the 30th cycle, which is superior than the capacity of the cathode materials prepared by other methods reported in the previous literatures [9, 28, 29]. The sample B (synthesized by the sol–gel method) shows a discharge capacity of 232 mA $hg^{-1}$, which is not as good as sample A.

In order to explore the reason of the capacity increasing with cycles, the differential capacity versus voltage curves of the $Li[Ni_{0.2}Li_{0.2}Mn_{0.6}]O_2$ cathode material synthesized by the "mixed oxalate" method cycled at 0.1 C in the voltage range of 2.5–4.8 V is shown in Fig. 6. The high oxidation peak at around 4.6 V in the first charge curves disappeared in the subsequent charges, meaning that the removal of lithium as "$Li_2O$" from the lattice only happens in the first cycle. As indicated in Fig. 6, the d$Q$/d$V$ curves plotted from different cycles show some differences, illustrating that some changes have happened in the cathode material as the cycles go on. The reduction peak below

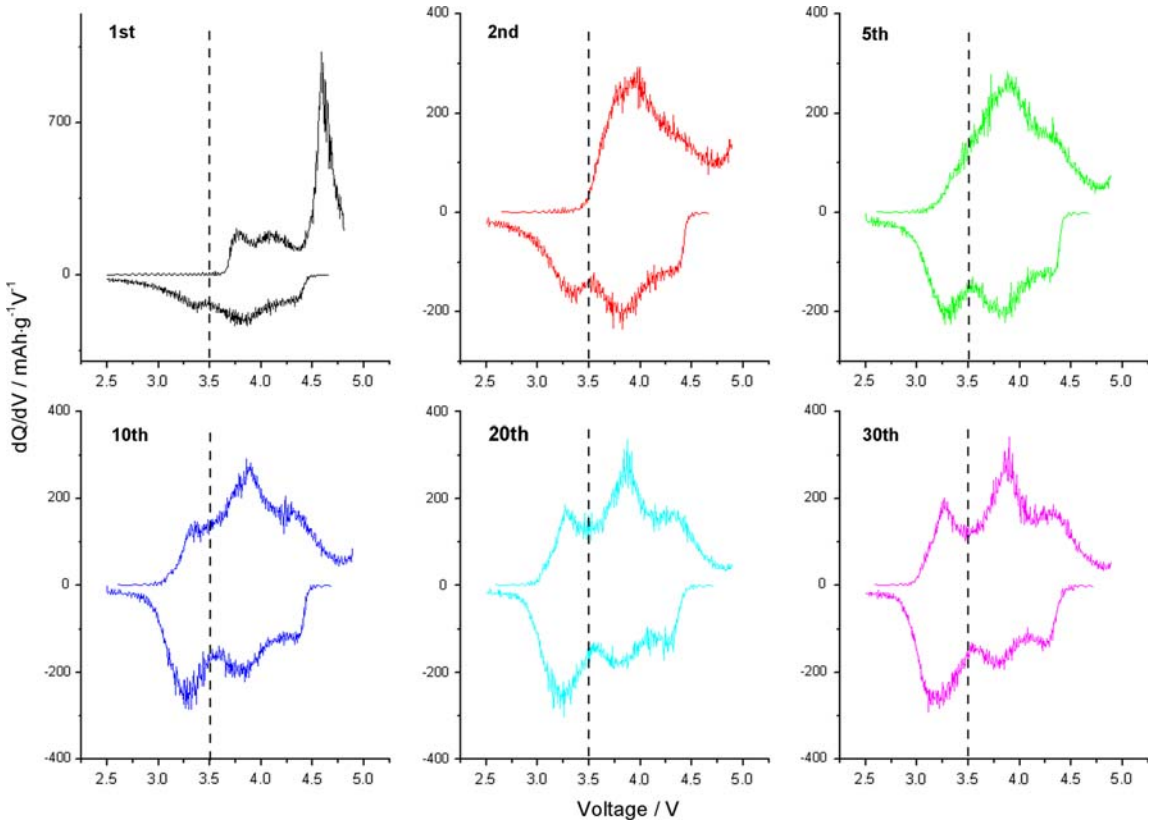


**Fig. 6** Differential capacity versus voltage curves at different cycles of the $Li[Ni_{0.2}Li_{0.2}Mn_{0.6}]O_2$ cathode material synthesized by the "mixed oxalate" method cycled at 0.1 C in the voltage range of 2.5–4.8 V

3.5 V, which can be assigned to the redox-reaction of $Mn^{4+}/Mn^{3+}$ [7], grows and becomes more evident. It is a signal that $Mn^{4+}$ in the cathode material becomes more and more active as the cycle number increases. As a result, more and more tetravalent Mn ions participate in the electrochemical reactions, and that is why, the discharge capacity increases with cycles [27].

## 4 Conclusions

In summary, this study introduces another choice—the "mixed oxalate" method to synthesize the Li-rich layered cathode material $Li[Ni_{0.2}Li_{0.2}Mn_{0.6}]O_2$. The structural and electrochemical properties of the sample synthesized by the "mixed oxalate" method are compared with the sample synthesized the sol–gel method. X-ray photoelectron spectroscopy (XPS) indicates that the valences of Ni and Mn in the cathode materials synthesized by the above two different methods are +2 and +4, respectively. X-ray diffraction (XRD) confirms that the Li, Ni, and Mn atoms in the transition metal layer of the structure are in the form of short-range ordered superlattice. The synthesized powders have a layered $O_3$–$LiCoO_2$-type structure with the *R-3m* symmetry. The results show that $Li[Ni_{0.2}Li_{0.2}Mn_{0.6}]O_2$ materials synthesized by the "mixed oxalate" method have a comparable electrochemical property with or even better than the electrochemical property of the sample synthesized by the sol–gel method. Its discharge capacity increases gradually from the initial value of 228 mA $hg^{-1}$ to a stable capacity of over 260 mA $hg^{-1}$ after the 10th cycle. It delivers a larger discharge capacity of 258 mA $hg^{-1}$ at the 30th cycle. The d*Q*/d*V* curves suggest that the increasing capacity results from the redox-reaction of $Mn^{4+}/Mn^{3+}$.

**Acknowledgments** We acknowledge the financial supports from the National Basic Research Program (2009CB220100) and BIT Basic Research Fund (No. 20070542004). We also would like to thank Dr. Guangyao Liu of Institute of Physics, Chinese Academy of Sciences, for his contribution to the Rietveld refinement of the XRD pattern.

## References

1. Numata K, Sakaki C, Yamanaka S (1999) Solid State Ion 117:257
2. Grincourt Y, Stoery C, Davidson IJ (2001) J Power Sour 97:711
3. Balasubramanian M, Mcbreen J, Davidson IJ et al (2002) J Electrochem Soc 149:A176
4. Lu ZH, MacNeil DD, Dahn JR (2001) Electrochem Solid State Lett 4:A191
5. Barkhouse DAR, Dahn JR (2005) J Electrochem Soc 152:A746
6. Johnson CS, Li N, Lefief C et al (2007) Electrochem Commun 9:787
7. Lu ZH, Dahn JR (2002) J Electrochem Soc 149:A815
8. Armstrong R, Holzapfel M, Bruce PG et al (2006) J Am Chem Soc 128:8694
9. Hwang BJ, Wang CJ, Chen CH et al (2005) J Power Sour 146:658
10. Lu Z, Dahn JR (2001) J Electrochem Soc 148:A237
11. Kim JS, Johnson CS, Vaughey JT et al (2004) Chem Mater 16:1996
12. Jiang J, Dahn JR (2005) Electrochim Acta 50:4778
13. Meng YS, Ceder G, Shao-Horn Y et al (2005) Chem Mater 17:2386
14. Cho TH, Park SM, Yoshio M et al (2005) J Power Sour 142:306
15. Kang YJ, Kim JH, Lee SW et al (2005) Electrochim Acta 50:4784
16. Lee KS, Myung ST, Moon JS et al (2008) Electrochim Acta 53:6033
17. Roisnel J, Rodriguez-Carjaval J (2000) Fullprof manual. Institut Laue-Langevin, Grenoble
18. Lu Z, Chen Z, Dahn JR (2003) Chem Mater 15:3214
19. Lu Z, Beaulieu LY, Donaberger RA (2002) J Electrochem Soc 149:A778
20. Hong YS, Park YJ, Ryu KS et al (2005) Solid State Ion 176:1035
21. Ryu JH, Park BJ, Park YJ et al (2009) J Appl Electrochem 39:1059
22. Liu HS, Li J, Zhang ZR et al (2004) Electrochim Acta 49:151
23. Carley AF, Jackson SD, O'Shea JN et al (1999) Surf Sci 440:L868
24. Yoncheva M, Stoyanova R, Zhecheva E et al (2009) J Alloys Compd 475:96
25. Sun Y, Shiosaki Y, Xia Y et al (2006) J Power Sour 159:1353
26. Yu L, Qiu W, Lian F et al (2008) Mater Lett 62:3010
27. Yu L, Qiu W, Lian F et al (2009) J Alloys Compd 471:317
28. Hong YS, Park YJ, Ryu KS et al (2004) J Mater Chem 14:1424
29. Yu LH, Yang HX, Ai XP et al (2005) J Phys Chem B 109:1148